

Hall Drag and Magnetodrag in Graphene

Justin C. W. Song^{1,2} and Leonid S. Levitov¹

¹ *Department of Physics, Massachusetts Institute of Technology, Cambridge, Massachusetts 02139, USA and*

² *School of Engineering and Applied Sciences, Harvard University, Cambridge, Massachusetts 02138, USA*

Massless Dirac fermions in graphene at charge neutrality form a strongly interacting system in which charge-neutral modes comprised of correlated particle-hole excitations play a dominant role. The neutral modes are essentially decoupled from charge dynamics in the absence of a magnetic field, but become strongly coupled to charge modes when a field is applied. We show that these ideas explain the recently observed giant magnetodrag, arising in classically weak fields when electron density in the layers is tuned near charge neutrality. We predict strong Hall drag in this regime, which is in stark departure from the weak coupling regime, where theory predicts the absence of Hall drag. Hall drag and magnetodrag arise in a wide temperature range and at classically weak magnetic fields, and feature an unusually strong dependence on field and carrier density.

Graphene near charge neutrality (CN) hosts an intriguing charge-compensated electron-hole system with unique properties. Theory predicts a number of interesting phenomena for this system: strong interactions and criticality[1–4], momentum-conserving collisions giving rise to finite resistivity in the absence of disorder[5–7]; strong thermopower resulting from coupling between charge modes and neutral modes[8–11]; anomalous thermodynamics[4] and new collective modes[12, 13]. Our understanding of the behavior at CN would benefit tremendously from introducing ways to efficiently couple the novel neutral modes predicted at CN to charge modes which can be easily probed in transport measurements. There is a long history, particularly in areas such as plasma physics and astrophysics, of employing magnetic field for such a purpose. The hydrodynamics of charge-neutral plasmas is ultra-sensitive to the presence of external magnetic fields. Further, dynamically generated magnetic fields can result in striking new phenomena, such as thermomagnetic waves, predicted in astrophysics[14] and later discovered in a 3D semimetal[15].

A new promising system in which magnetotransport at CN can be probed are atomically thin graphene-based heterostructures[16, 17]. In these systems, strong Coulomb coupling between adjacent layers leads to strong interlayer correlations. A striking manifestation of these correlations is provided by Coulomb drag[17–25], in which current applied in one (active) layer induces a voltage in the adjacent (passive) layer. Strong interactions manifest themselves in a drag resistance that peaks near CN [17]. Interestingly, the measurements [17] revealed dramatic magnetic field dependence, with the drag resistivity at CN increasing by more than an order of magnitude (and changing sign) upon application of a relatively weak B field. In particular, for fields as low as $B \sim 0.1$ T the longitudinal drag at CN features a five-fold increase as compared to drag at $B = 0$ [17]. Strong magnetic field dependence of drag has been observed previously in other double layer two-dimensional electron gas (2DEG) heterostructures[26–28], however these experiments were carried out in the quantum Hall regime,

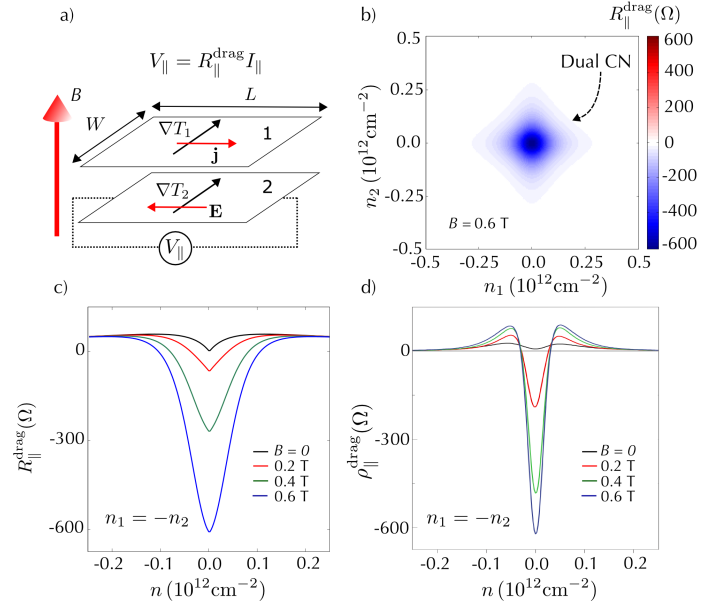


FIG. 1: Magnetodrag in a double layer graphene heterostructure in the presence of a finite magnetic field. (a) Schematic of charge current, temperature gradients, and electric field in the two layers. (b,c) Predicted density dependence of magnetodrag resistance, $R_{||}^{drag}$, from Eq.(12) and Eq.(14). Parameter values: $B = 0.6$ T, $n_0 = 10^{11} \text{ cm}^{-2}$, $T = 150$ K, and $\rho_0 = \frac{h}{3e^2}$. The $B = 0$ dependence taken from the model of drag at zero B field [24, 25]. (d) Experimentally measured magnetodrag resistivity in G/hBN/G heterostructures, reproduced from Ref. [17] for the same B values as in (c). Application of magnetic field leads to a giant increase of drag at CN. Note the similarity between data and theoretically predicted drag density dependence, B dependence, and sign.

whereas the anomalous magnetodrag found in Ref. [17] occurs at classically weak fields $B \lesssim 1$ T. This puzzling behavior, which is not yet understood, will be explained below (see Fig.1).

Another outstanding question that magnetodrag measurements may help settle is that of Hall drag. It has long been debated whether a Hall voltage can arise in the passive layer in the presence of a DC current in the active

layer [29, 30]. In particular, theory predicts a *vanishing* Hall drag [29, 30]. This is because transferred momentum is parallel to velocity, allowing only a longitudinal “back-current” to develop in the passive layer. As discussed below, this conclusion is valid only in the weak coupling regime. At strong coupling, charge and energy transport become dominated by long-range neutral modes, which in our system is described by electron-lattice temperature imbalance. At CN, the magnitude of the cross-couplings between charge and energy currents becomes large, producing a finite Hall drag

$$V_H = R_H^{\text{drag}} I_{\parallel}. \quad (1)$$

Our theory predicts R_H^{drag} values which are consistent with observations[31] but orders of magnitude greater than those observed in earlier experiments (see below).

The flow of charge and energy, which are completely decoupled in the absence of magnetic field (in a spatially uniform system), become strongly coupled in the presence of a magnetic field. As we will see, the effects arising due to such coupling dominate Coulomb drag at CN. Heat current and an electric field, induced by charge current and temperature gradients, are coupled via the thermoelectric effect altered by the B field,

$$\mathbf{j}_q = \underline{\mathbf{Q}}\mathbf{j}, \quad \mathbf{E} = \underline{\mathbf{Q}} \frac{\nabla T}{T}. \quad (2)$$

Here $\underline{\mathbf{Q}}$ is a 2×2 matrix, of which diagonal components describe the Peltier and Thompson effects, and off-diagonal components describe the Nernst-Ettingshausen effect. Crucially, vertical energy transfer between layers does not discriminate between longitudinal and transverse heat currents since temperature profile is a scalar field. This stands in contrast to conventional momentum driven drag, where momentum transfer is parallel to the applied current [29, 30]. As illustrated in Fig. 1a, when a longitudinal charge current is applied in the active layer (for $B \neq 0$) a transverse (Ettingshausen) heat current develops in both layers through efficient vertical energy transfer. Nernst voltage in the passive layer results in a longitudinal magnetodrag (see Fig. 1b,c). The resulting density and field dependence strongly resembles the observed magnetodrag[17], reproduced in Fig. 1d.

As we will see below, this mechanism also leads to Hall drag. As illustrated in Fig.1 and Fig.2, we find Hall and magnetodrag resistances, R_H^{drag} and $R_{\parallel}^{\text{drag}}$, that are large and peak near CN. As we will see, these large values arise even for classically weak fields $B \sim 0.1$ T. Indeed, both R_H^{drag} and $R_{\parallel}^{\text{drag}}$ exceed by *two orders of magnitude* those found previously in GaAs/AlGaAs 2DEG heterostructures [26–28] at similar fields. Additionally, both quantities exhibit sharp growth as a function of B . The steep differential magnetodrag resistance can be used in sensitive field and temperature sensing applications.

In our analysis we will focus on a Hall-bar geometry of two parallel rectangular layers of dimensions $L \times W$,

pictured in Fig.1a. For the sake of simplicity, we treat the electric and heat currents as independent of the x coordinate along the bar. In layer 1, current is injected at $x = -L/2$ and drained at $x = L/2$. In layer 2, the Hall drag voltage arising across the device, V_H and the longitudinal drag voltage, V_{\parallel} , are evaluated as

$$V_H = \int_{-W/2}^{W/2} E_y^{(2)} dy, \quad V_{\parallel} = \frac{L}{W} \int_{-W/2}^{W/2} E_x^{(2)} dy \quad (3)$$

The electric and thermal variables may depend on the transverse coordinate y , reflecting thermal coupling between the two layers.

To obtain the electric field in layer 2 induced by current applied in layer 1, we first need to understand the coupling of temperature profiles $T_{1,2}(\mathbf{r})$ in the two layers. Energy transport in the system can be described by

$$\begin{aligned} -\nabla \kappa_1 \nabla \delta T_1 + a(\delta T_1 - \delta T_2) + \lambda \delta T_1 &= -\nabla \cdot (\underline{\mathbf{Q}}^{(1)} \mathbf{j}) \\ -\nabla \kappa_2 \nabla \delta T_2 + a(\delta T_2 - \delta T_1) + \lambda \delta T_2 &= 0 \end{aligned} \quad (4)$$

where a is the energy transfer rate between the two layers [25], λ is the electron-lattice cooling rate, and $\delta T_i = T_i - T_0$. Here T_0 is the lattice temperature of the two layers.

The boundary conditions are given by the condition of electric current being tangential to the free boundaries at $y = \pm W/2$, and zero temperature imbalance at the Hall-bar ends, $x = \pm L/2$, since the current and voltage contacts act as ideal heat sinks. The electric current parallel to the boundaries $y = \pm W/2$ gives rise to the Ettingshausen heat current that may have a component transverse to the Hall bar. The divergence of this heat current, appearing on the right hand side of Eq.(4), acts as an effective boundary delta function source in the heat transport equations.

We consider the case of a spatially uniform $\underline{\mathbf{Q}}$ in both layers. The ideal heat sinks at $x = \pm L/2$ mean that no temperature imbalance develops in the x -direction (except for some “fringing” heat currents near the contacts which give a contribution small in W/L , we will ignore these fringing currents in the following discussion). Indeed far away from these contacts, no temperature gradients are sustained in the x -direction and we reduce our problem Eq. (4) to a quasi-one dimensional problem with temperature profiles that only depend on the y -coordinate for $W < L$. As a result, the only heat source arises from the Ettingshausen effect $\underline{\mathbf{Q}}^{(1)} \mathbf{j} = (Q_{yx}^{(1)} \hat{y}) \hat{y}$.

To describe transport in the presence of such a source, we will expand temperature variables in both layers in a suitable orthonormal set of functions. Here it will be convenient to use eigenstates of the operator ∂_y^2 with zero Neumann boundary conditions at $y = \pm W/2$, given by

$$u_n(y) = A \cos\left(\frac{2\pi n}{W} y\right), \quad v_n(y) = A \sin\left(\frac{2\pi(n + \frac{1}{2})}{W} y\right),$$

$A = (2/W)^{1/2}$, $n = 0, 1, 2, \dots$. From the symmetry of the source in Eq.(4) we expect $\delta T_{1,2}(y)$ to be odd in y . Thus

only the functions $v_n(y)$ are relevant, giving

$$\delta T_{1,2}(y) = \sum_{q_n} \delta \tilde{T}_{1,2}(q_n) A \sin q_n y, \quad q_n = \frac{2\pi(n + \frac{1}{2})}{W}.$$

For each n we obtain a pair of algebraic equations

$$\begin{aligned} q_n^2 \kappa_1 \delta \tilde{T}_1 + a(\delta \tilde{T}_1 - \delta \tilde{T}_2) + \lambda \delta \tilde{T}_1 &= F_n \\ q_n^2 \kappa_2 \delta \tilde{T}_2 + a(\delta \tilde{T}_2 - \delta \tilde{T}_1) + \lambda \delta \tilde{T}_2 &= 0 \end{aligned} \quad (5)$$

where $\kappa_{1,2} = \kappa_{xx}^{(1,2)}$ and $F_n = 2A(-1)^n Q_{yx}^{(1)} j$. Solving Eq.(5), we find the temperature profile in layer 2:

$$\delta T_2(y) = \sum_{n \geq 0} \frac{a F_n}{L_1(q_n) L_2(q_n) - a^2} v_n(y), \quad (6)$$

where $L_i(q_n) = \kappa_i q_n^2 + a + \lambda$ ($i = 1, 2$). Since electron-lattice cooling is very slow [32, 33], with the corresponding cooling length values in excess of few microns, we will suppress λ in what follows. Because the boundaries in the transverse (y -direction) are free, a finite temperature imbalance between the edges can arise, given by $\Delta T = \delta T_2(y = W/2) - \delta T_2(y = -W/2)$. We find

$$\Delta T = 4A^2 \sum_{n \geq 0} \frac{a Q_{yx}^{(1)} j}{L_1 L_2 - a^2} = \frac{8}{W \tilde{\kappa}} \sum_{n \geq 0} \frac{Q_{yx}^{(1)} j}{q_n^2 (1 + \xi^2 q_n^2)}, \quad (7)$$

where we defined $\tilde{\kappa} = \kappa_1 + \kappa_2$ and a length scale $\xi = \sqrt{\kappa_1 \kappa_2 / a \tilde{\kappa}}$. We evaluate the sum using the identity

$$\sum_{n=0}^{\infty} \frac{1}{(n + \frac{1}{2})^4 + c^2 (n + \frac{1}{2})^2} = \frac{\pi^2}{2c^2} \left(1 - \frac{\tanh \pi c}{\pi c} \right)$$

to obtain

$$\Delta T = \frac{W Q_{yx}^{(1)} j}{\tilde{\kappa}} G(\xi), \quad G(\xi) = 1 - \frac{2\xi}{W} \tanh \left(\frac{W}{2\xi} \right). \quad (8)$$

Connecting ΔT with the drag voltage, and in particular determining its sign, requires taking full account of Onsager reciprocity. This analysis is presented below.

In the same way that the applied charge current, \mathbf{j} , in layer 1 causes a heat current (Peltier/Ettingshausen), a temperature imbalance in layer 2, ΔT , can sustain voltage drops across the sample (Thermopower/Nernst). These two effects are related by Onsager reciprocity constraints. The cross couplings in the coupled energy and charge transport equations [34] arise from

$$\begin{pmatrix} -\mathbf{j} \\ \mathbf{j}_q \end{pmatrix} = \begin{pmatrix} e \mathbf{L}_{11}/T & e \mathbf{L}_{12} \\ \mathbf{L}_{21}/T & \mathbf{L}_{22} \end{pmatrix} \begin{pmatrix} \nabla \mu \\ \nabla \frac{1}{T} \end{pmatrix} \quad (9)$$

where \mathbf{L} are 2×2 matrices and e is the carrier charge. In this notation, the electrical conductivity equals $\underline{\sigma} = e^2 \mathbf{L}_{11}/T$, and thermal conductivity is $\underline{\kappa} = \mathbf{L}_{22}/T^2$. Comparing to the heat current due to an applied charge current, Eq.(2), we identify $\mathbf{L}_{21} = -e \mathbf{Q} \mathbf{L}_{11}$.

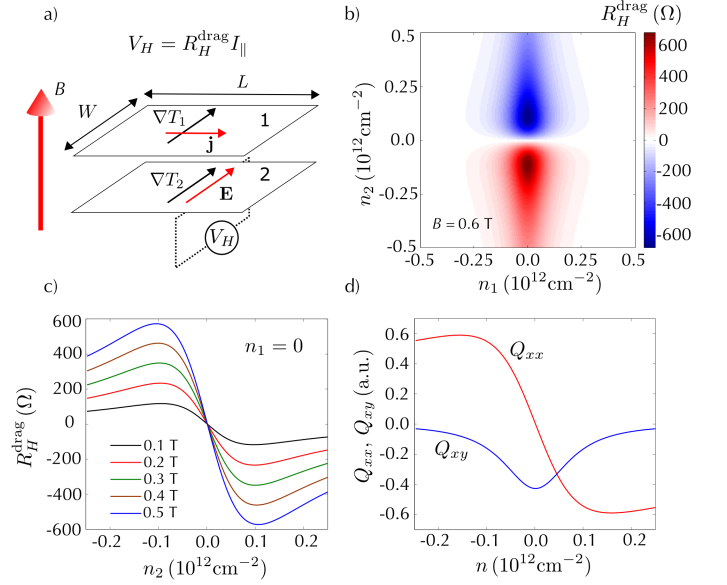


FIG. 2: Hall drag in a graphene heterostructure in the presence of a magnetic field. (a) Schematic of charge current, temperature gradients, and electric field in the two layers. (b,c) Density dependence of Hall drag resistance, predicted from Eq.(12) and Eq.(14) for the same parameter values as in Fig.1. (d) Density dependence of Q_{xx} , Q_{xy} , see text.

Onsager reciprocity demands that the cross-couplings obey $\mathbf{L}_{12}(B) = \mathbf{L}_{21}^T(-B)$ where B is the applied magnetic field (note the transposed matrix). In an isotropic system the off-diagonal components of \mathbf{L} obey $\mathbf{L}^{(xy)}(B) = \mathbf{L}^{(yx)}(-B)$. As a result, Onsager reciprocity reduces to

$$\mathbf{L}_{12}(B) = \mathbf{L}_{21}(B) \quad (10)$$

in an isotropic system. Applying Eq. 10 to Eq. 9 in an open circuit, we find $\mathbf{E} = -e^{-1} \nabla \mu = T^{-1} \mathbf{L}_{11}^{-1} \mathbf{Q} \mathbf{L}_{11} \nabla T$. For an isotropic system $\mathbf{Q} = Q_{xx} \mathbf{1} - i Q_{xy} \sigma_2$, $\mathbf{L} = L_{xx} \mathbf{1} - i L_{xy} \sigma_2$, so that $[\mathbf{Q}, \mathbf{L}] = 0$, which gives Eq.(2).

Using Eq.(3) and Eq.(2) we obtain

$$\begin{pmatrix} V_{\parallel} \\ V_H \end{pmatrix} = \begin{pmatrix} R_{\parallel}^{\text{drag}} & -R_H^{\text{drag}} \\ R_H^{\text{drag}} & R_{\parallel}^{\text{drag}} \end{pmatrix} \begin{pmatrix} I_{\parallel} \\ 0 \end{pmatrix}, \quad (11)$$

giving the magnetodrag and Hall drag resistance values

$$R_H^{\text{drag}} = \frac{-G(\xi)}{T \tilde{\kappa}} Q_{xy}^{(1)} Q_{xx}^{(2)}, \quad R_{\parallel}^{\text{drag}} = \frac{-LG(\xi)}{WT \tilde{\kappa}} Q_{xy}^{(1)} Q_{xy}^{(2)}. \quad (12)$$

Here we have used the fact that in an isotropic system $Q_{xx} = Q_{yy}$ and $Q_{xy} = -Q_{yx}$. When $\xi/W \ll 1$, we have $G \rightarrow 1$ so that $R_{H,\parallel}^{\text{drag}}$ saturates to become independent of the the energy transfer rate between the two layers, a . However, when $\xi/W \gg 1$, we have $G \rightarrow 0$ so that $R_{H,\parallel}^{\text{drag}}$ vanish with decreasing energy transfer rate, a .

To describe the density and B field dependence, we use a simple model for \mathbf{Q} . Measurements indicate[8, 9] that thermopower and the Nernst effect in graphene are well

described by the Mott formula [35], giving

$$Q_{ms} = \frac{\pi^2}{3e} k_B^2 T^2 \sum_k \rho_{mk} \frac{\partial[\rho^{-1}]_{ks}}{\partial \mu} \quad (13)$$

where ρ is the magneto-resistance and μ is the chemical potential. Here we concentrate on classically weak magnetic fields relevant for recent experiments [17]. We model the tensor $\rho = \begin{pmatrix} \rho_{\parallel} & \rho_H \\ -\rho_H & \rho_{\parallel} \end{pmatrix}$ as follows:

$$\rho_{\parallel} = \frac{\rho_0}{\sqrt{1 + n^2/n_0^2}}, \quad \rho_H = \frac{-Bn}{e(n^2 + n_0^2)^2}, \quad (14)$$

where ρ_0 is the resistivity peak at the Dirac point, n is the carrier density, and parameter n_0 accounts for broadening of the Dirac point due to disorder. We account for disorder broadening of the density of states, $dn/d\mu = (n^2 + n_0^2)^{1/4} (2/(\pi\hbar^2 v_F^2))^{1/2}$.

Using Eqs.(12),(13),(14) we obtain $R_{\parallel}^{\text{drag}}$ (in Fig.1b,c) and R_H^{drag} (in Fig.2b,c). In that, we used the parameter values $n_0 = 10^{11} \text{ cm}^{-2}$, $\rho_0 = \frac{\hbar}{3e^2}$, and a representative temperature, $T = 150 \text{ K}$. These values match the characteristics (disorder broadening, n_0 , and peak resistivity, ρ_0) of G/hBN heterostructures described in Ref.[17]. As a sanity check, we plot the components of \mathbf{Q} (in Fig.2d) which show the behavior near CN matching thermopower and Nernst effects measured in graphene[8, 9].

Plotting magnetodrag in Fig. 1b, we find $R_{\parallel}^{\text{drag}}$ peaks at dual CN showing a *giant* and *negative* trans-resistance. At its peak, $R_{\parallel}^{\text{drag}}$ is two orders of magnitude larger than magnetodrag measured in GaAs quantum wells [26–28] where drag resistivities of several ohms were seen at similarly weak fields. Magnetodrag in Fig. 1c exhibits a steep B dependence, $R_{\parallel, \text{peak}}^{\text{drag}} \propto -B^2$, that bears a striking resemblance to measurements in Ref.[17] reproduced in Fig.1d. In particular, our model explains the negative sign of the measured magnetodrag peak.

Hall drag, shown in Fig.2b,c, is large and sign-changing. Finite R_H^{drag} is a ‘smoking gun’ of strong coupling to the neutral modes at CN in graphene (see Fig. 2a). Already for classically weak magnetic fields, $B \lesssim 0.1 \text{ T}$, this strong coupling manifests in a giant R_H^{drag} of several hundred ohms (Fig. 2c). This is two orders of magnitude larger than the few-ohm Hall drag resistance measured in GaAs quantum wells [26] at similar fields. R_H^{drag} also exhibits dependence on magnetic field, with peak heights increasing linearly with B (Fig.2c). Interestingly, only carrier density in layer 2 controls the sign of R_H^{drag} , breaking the $n_1 \leftrightarrow n_2$ symmetry between layers - a unique signature of Hall drag in graphene.

In summary, magnetic field has a strong impact on drag at CN because it induces strong coupling between neutral and charge modes, which are completely decoupled in the absence of an applied magnetic field in a uniform system. Field-induced mode coupling leads to

giant drag that dwarfs the conventional momentum drag contribution as well as a remnant drag due to spatial inhomogeneity[25]. Our estimates indicate that these two contributions are orders of magnitude smaller than the predicted magnetodrag, which also has an opposite sign. The giant magnetodrag and Hall drag values attained at classically weak magnetic fields, along with the unique density dependence and sign, make these effects easy to identify in experiment. The predicted magnetodrag is in good agreement with findings in Ref.[17]. Magnetic field, coupled with drag measurements at CN, provides a unique tool for probing the neutral modes in graphene.

We acknowledge useful discussions with A. K. Geim, P. Jarillo-Herrero, L. A. Ponomarenko, and financial support from the NSS program, Singapore (JS).

-
- [1] J. Gonzales, F. Guinea, and M.A.H. Vozmediano, Nucl. Phys. B **424**, 595 (1994); Phys. Rev. B **59**, R2474 (1999).
 - [2] D. E. Sheehy and J. Schmalian Phys. Rev. Lett. **99**, 226803 (2007).
 - [3] D. T. Son Phys. Rev. B **75**, 235423 (2007).
 - [4] O. Vafek, Phys. Rev. Lett. **98**, 216401 (2007).
 - [5] A. B. Kashuba, Phys. Rev. B **78**, 085415 (2008).
 - [6] L. Fritz, J. Schmalian, M. Mueller, S. Sachdev, Phys. Rev. B **78**, 085416 (2008).
 - [7] M. Mueller, L. Fritz, S. Sachdev, Phys. Rev. B **78**, 115406 (2008).
 - [8] Y. M. Zuev, W. Chang, and P. Kim, Phys. Rev. Lett. **102**, 096807 (2009).
 - [9] P. Wei, W. Bao, Y. Pu, C. N. Lau, and J. Shi, Phys. Rev. Lett. **102**, 166808 (2009).
 - [10] J. G. Checkelsky and N. P. Ong, Phys. Rev. B **80**, 081413(R) (2009).
 - [11] E. H. Hwang, E. Rossi, and S. Das Sarma Phys. Rev. B **80**, 235415 (2009).
 - [12] O. Vafek, Phys. Rev. Lett. **97**, 266406 (2006)
 - [13] S. Gangadharaiah, A. M. Farid, and E. G. Mishchenko Phys. Rev. Lett. **100**, 166802 (2008).
 - [14] L. E. Gurevich, B. L. Gelmont, Zh. Eksp. Teor. Fiz. **51**, 183 (1966) [Sov. Phys. JETP **24**, 124 (1967)]; Sov. Astronomy **11**, 609 (1968).
 - [15] V. N. Kopylov, JETP Lett **28**, 121 (1978).
 - [16] L. Britnell, *et al.* Science **335**, 947 (2012).
 - [17] R. V. Gorbachev, *et al.* Nature Physics **8**, 896 (2012).
 - [18] S. Kim, I. Jo, J. Nah, Z. Yao, S. K. Banerjee, and E. Tutuc, Phys. Rev. B **83**, 161401 (2011).
 - [19] W.-K. Tse and S. Das Sarma, Phys. Rev. B **75**, 045333 (2007).
 - [20] B. N. Narozhny, Phys. Rev. B **76**, 153409 (2007).
 - [21] E. H. Hwang, R. Sensarma, and S. Das Sarma, Phys. Rev. B **84**, 245441 (2011).
 - [22] N. M. R. Peres, J. M. B. Lopes dos Santos, and A. H. Castro Neto, Europhys. Lett. **95**, 18001 (2011).
 - [23] M. I. Katsnelson, Phys. Rev. B **84**, 041407 (2011).
 - [24] B. N. Narozhny, M. Titov, I. V. Gornyi, and P. M. Ostrovsky, Phys. Rev. B **85**, 195421 (2012).
 - [25] J. C. W. Song and L. S. Levitov, Phys. Rev. Lett. **109**, 236602 (2012).
 - [26] N. K. Patel, E. H. Linfield, K. M. Brown, M. Pepper, D. A. Ritchie, and G. A. C. Jones, Semicond. Sci. Technol.,

- 12**, 309 (1997).
- [27] H. Rubel, A. Fischer, W. Dietsche, K. von Klitzing, and K. Eberl, Phys. Rev. Lett. **78** 1763 (1997).
 - [28] M. P. Lilly, J. P. Eisenstein, L. N. Pfeiffer, and K. W. West, Phys. Rev. Lett., **80** 1714 (1998).
 - [29] A. Kamenev and Y. Oreg, Phys. Rev. B, **52** 7516 (1995).
 - [30] M. C. Bonsager, K. Flensberg, B. Y.-K. Hu, and A.-P. Jauho, Phys. Rev. Lett., **77** 1366 (1996). The authors note that Hall drag vanished for systems with inversion symmetry and when the carriers in the active layer can be described by a drifted Fermi-Dirac distribution.
 - [31] A. K. Geim, private communication
 - [32] M. W. Graham, S-F. Shi, D. C. Ralph, J. W. Park, P. L. McEuen, Nature Physics, **9** 103 (2013)
 - [33] A. C. Betz, S. H. Jhang, E. Pallecchi, R. Ferreira, G. Fève, J-M. Berroir, and B. Placais, Nature Physics, **9** 109 (2013).
 - [34] H. B. Callen, Phys. Rev., **73** 1349 (1948).
 - [35] M. Jonson and S. M. Girvin, Phys. Rev. B, **29** 1939 (1984).